Journal of Sol-Gel Science and Technology (2021) 97:340–350
https://doi.org/10.1007/s10971-020-05446-1

ORIGINAL PAPER: SOL-GEL AND HYBRID MATERIALS FOR CATALYTIC, PHOTOELECTROCHEMICAL AND SENSOR APPLICATIONS

Amylases encapsulated in organosilane-modified silicas prepared by sol–gel: evaluation of starch saccharification

José Rodrigo Fernandez Caresani[1] · Alexsandro Dallegrave[2] · João Henrique Zimnoch Dos Santos[2]

Received: 28 April 2020 / Accepted: 17 November 2020 / Published online: 7 January 2021

Abstract

A series of amylases were encapsulated within silica matrices taking into account the nature of the amylase: α-amylase (*Bacillus subtilis*), α-amylase (*Aspergillus oryzae*), and β-amylase (barley), and the nature of the organosilane (alkyl-, amine- and mercaptan-based organosilanes). The results for the biocatalytic activity were shown to be dependent on the nature of the encapsulated enzymes and on the nature of the employed organosilane. Organosilanes containing the amine group showed different effects and lower biocatalytic conversions (on average). In general, β-amylase increased in biocatalytic activity after encapsulation. There was a strong correlation between the nature of the organosilane and the resulting porosity of the matrix as well as the reducing sugars produced from the saccharification tests. The lower the particle radius of gyration and the higher degree ramification of the secondary particles, the higher the catalyst bioactivity was. Generally, glucose production during saccharification was favored by the encapsulation of the enzyme.

Graphical Abstract

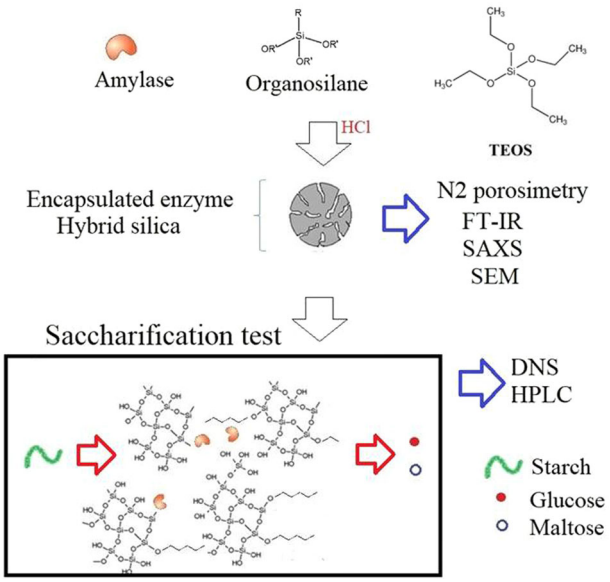

Supplementary information The online version of this article (https://doi.org/10.1007/s10971-020-05446-1) contains supplementary material, which is available to authorized users.

✉ João Henrique Zimnoch Dos Santos
jhzds@iq.ufrgs.br

[1] Departamento de Engenharia Química, Universidade Federal do Rio Grande do Sul, Rua Eng. Luis Englert s/n, Porto Alegre, Rio Grande do Sul 90040-040, Brasil

[2] Instituto de Química, Universidade Federal do Rio Grande do Sul, Porto Alegre, Rio Grande do Sul, Brasil

Keywords Sol–gel · Amylase · Hybrid silicas · Encapsulation · Saccharification

Highlights

- Different organosilanes (7) were employed to modify silica surface.
- The organosilanes containing the amine group showed lower bioconversion.
- β-amylase increased in biocatalytic activity after encapsulation.
- Organosilanes increase the pore diameter.

1 Introduction

Despite several decades of research devoted to the immobilization of enzymes, the quest for more active, selective, and robust-supported systems is still a present theme. The use of immobilized enzymes is now a routine process for the manufacture of many products in the pharmaceutical, chemical, and food industries. In general, all enzymatic reactions can benefit from immobilization. Nevertheless, the final choice to use enzymes in immobilized forms depends on the economic evaluation of the costs associated with their use versus the benefits obtained in the process [1, 2]. Strategies for efficient enzyme immobilization continue to be developed alongside the expanding number of available biocatalysts [3].

In recent years, the immobilization of enzymes that degrade some kind of substrate has continued to be the focus of several studies. For instance, the immobilization of β-galactosidase (*Aspergillus oryzae*) was applied to the hydrolysis of lactose into glucose and galactose [4]. Coimmobilized α-amylase and glucoamylase afforded a biocatalyst system that exhibited a higher rate of hydrolysis of starch from corn, rice, wheat, and potato than a free (not-immobilized) mixture of the enzymes [5]. A tri-enzyme biocatalyst (α-amylase, glucoamylase, and pullulanase) was prepared by cross-linking and aggregation. The catalyst activity of the immobilized enzymes was maintained after five cycles without any damage [6].

Among the different approaches employed in the immobilization of enzymes, one that has to be highlighted is the encapsulation method, which consists of the inclusion of an enzyme within a polymer network, such as organic or inorganic (silica) polymers and membrane (hollow-fiber), micro- or nanocapsules, chemically modified with metals or organic moieties [7–11]. Nevertheless, it is worth noting that encapsulation may suffer from some critical drawbacks, most of them intrinsic to heterogeneous catalysis, such as high mass transfer resistance to the substrate [12], enzyme leaching, hindrance of the access of the substrate to the catalytic center, and even catalyst loss during the encapsulation process [13].

The sol–gel process represents a versatile tool for the encapsulation of enzymes. This process involves essentially two reactions: hydrolysis and condensation, most commonly, of metal alkoxides, which can be tuned by the use of an acidic or basic catalyst [14]. When encapsulating enzymes using the sol–gel technique, it is necessary to take into account some aspects, such as avoiding hindering/blocking the active site (catalyst center) [15], avoiding enzyme denaturing due to experimental conditions (pH, temperature, etc.), and substrate diffusion through the encapsulating matrix.

Among the enzyme-processed raw materials, starch represents a relevant substrate. Starch is a mixture of glycans that plants synthesize as an energy reserve. It is composed of α-amylose and amylopectin. α-amylose is a linear polymer of thousands of glucose residues joined by α $(1 \rightarrow 4)$ bonds adopting an irregularly aggregated helix conformation. Amylopectin consists mainly of glucose residues joined by α $(1 \rightarrow 4)$ bonds but is a highly branched molecule with α branch points $(1 \rightarrow 6)$. Amylopectin molecules contain up to 10^6 glucose residues, making them some of the largest molecules present in nature [16]. The most stable three-dimensional structure for the α $(1 \rightarrow 4)$ bonded chains of starch is a tightly wound helix stabilized by hydrogen bonds between the chains forming the amylose helical structure [14].

In the literature, several examples report the immobilization of amylase in different matrices. For instance, examples specifically involving sol–gel processes are presented as follows: The encapsulation of *Aspergillus oryzae PP* (which has the capacity to produce amylase) within silica-based matrix produced by the sol–gel process (in combination with starch, ethylene oxide, calcium alginate) has shown that the activity of the encapsulated cell culture exhibited comparable activity with the free cell cultures [17]. Conversely, alpha-amylase immobilization within guar gum-silica nanohybrid material showed significantly higher bioactivity than free amylase in solution. The immobilized enzyme revealed that immobilization increased the overall catalytic property of the enzyme [18].

Despite several advances in amylase immobilization, there are still restrictions that need to be overcome. One of the most frequent problems in gel solution encapsulation of amylases is the diffusion of organic compounds (substrate) in the generated confinement matrix. In fact, one may

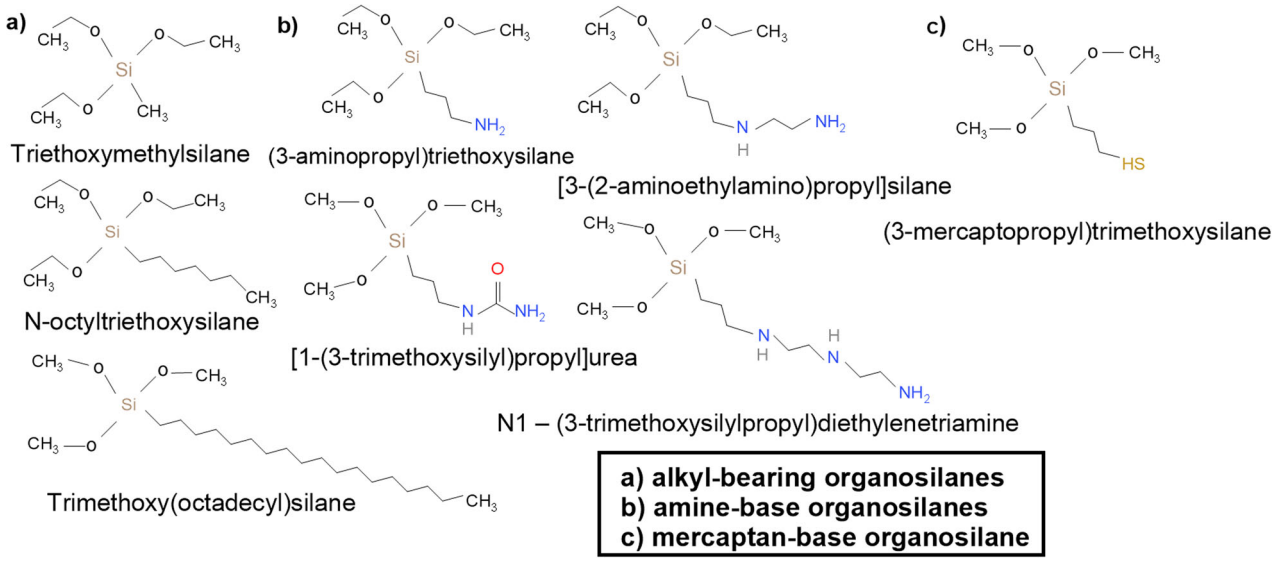

Scheme 1 Employed organosilanes, classified into three groups: **a** alkyl-bearing organosilane; **b** amine-based organosilanes, and **c** mercaptan-based organosilane

consider this problem intrinsic to immobilized catalysts. The limitations to the immobilization of amylases in a silica matrix may be associated with the large size and shape of the substrate itself, which has to migrate through the pores up to the active centers. Comparative study of enzymes other than amylase also points to matrix diffusion problems. The relative activities of the encapsulated enzymes, with respect to the free enzymes (in solution), were 20% for α-amylase and up to 57% for catalase. The lower performance of the former was probably due to the slow diffusion of the large substrate molecules (starch) within silica. In the case of catalase, optimal results were obtained after washing the gel with a Triton X-100 solution. Indeed, the surfactant treatment was indispensable to avoiding progressive blocking of the enzyme active sites during repeated uses of the same gel [19].

The versatility of the sol–gel, which dispose the possibility of several experimental routes, several precursors, and countless proportions of them, is extended in this work by including organosilanes with different functional groups which may allow to evaluate the influence of the chains in the matrix and the interaction of the groups of the enzymes with the functional groups of organosilanes in the alkyl chain.

In a previous study, the effects of pH, enzyme amount, and temperature both in free and silica-encapsulated amylases, namely, bacterial α-amylase (*Bacillus subtilis*), fungal α-amylase (*Aspergillus oryzae*), and β-amylase (barley), on the biocatalytic activity of the enzymes in terms of the content of reducing sugars were evaluated [20]. As an extension of this research, the present study aimed to investigate the role of several organosilanes (Scheme 1) added during the hydrolytic acid-catalyzed sol–gel encapsulation process. The organosilanes were classified into three groups: (a) alkyl-bearing organosilanes, (b) amine-based organosilanes, and (c) mercaptan-based organosilanes.

The introduction of organosilanes bearing different chemical moieties (polar and apolar chemical groups) aimed to investigate the role of such organic groups in the textural and structural characteristics of the resulting encapsulated enzymes and their influence on the biocatalytic activity in starch degradation (saccharification) as well as in the relative production of glucose and maltose. We estimated that the use of such organosilanes bearing different chemical functions may either interact with the catalyst center (as in the case of nitrogen-bearing compounds) or affect diffusion along the particle (as in the case of long-alkyl-chain organosilane). It is worth noting that the immobilization within a silica-based matrix produced by sol–gel may render the catalytic system more stable. On the other hand the rigid structure may affect diffusion through silica structure. The hypothesis of this research is that the use of organosilanes in the sol–gel process would affect the texture of the grain, besides the functional groups could interact with the enzymes, tuning activity, and selectivity.

2 Experimental procedures

2.1 Materials

Isopropyl alcohol (99.5%—Dinâmica), TEOS (tetraethylorthosilicate) (98%—Sigma-Aldrich), buffer solution

(aqueous solution containing $CaCl_2$ and sodium acetate—pH = 6.7), hydrochloric acid (37%—Synth), and water were employed in the sol–gel synthesis. Silica chemical modification was carried out with the following compounds: C1 (triethoxymethylsilane) (99%—Sigma-Aldrich), C8 (N-octyltriethoxysilane) (Dow Corning), C18 (trimethoxy(octadecyl)silane) (TCI—≥85%), (3-aminopropyl)triethoxysilane (99%—Sigma-Aldrich), [1-(3-trimethoxysilyl)propyl]urea (99%—Sigma-Aldrich), [3-(2-aminoethylamino)propyl]silane (>80—Sigma-Aldrich), N1-(3-trimethoxysilylpropyl)diethylenetriamine, and (3-mercaptopropyl)trimethoxysilane. α-amylase from *Bacillus subtilis* (55.6 U/mg), α-amylase from *Aspergillus oryzae* (>800 FAU/g), and β-amylase from barley (53 U/mg) were purchased from Sigma-Aldrich. For the starch saccharification process and the DNS (3,5-dinitrosalicylic acid (DNS)) method, the following reagents were used: glucose (>99.5%—Neon), soluble starch (99%—Dynamic), phenol (99%—Dynamic), potassium tartrate (99%—Dynamic), sodium metabisulfite (97%—NEON), DNS (98%—Sigma-Aldrich), citric acid (99.5%—NEON), and sodium bibasic phosphate (98%—NEON). The glucose and maltose standards used for high-performance liquid chromatography (HPLC) (>99%) were also purchased from Sigma-Aldrich. Isopropyl alcohol has less denaturing power than conventional ethanol.

2.2 Enzyme immobilization

In a typical preparation, 5 mL of TEOS, 3 mL of isopropyl alcohol, 20 mL of deionized water, 1 mL HCl (0.01 N) (acid catalyst), and 0.35-mL buffer solution (sodium acetate and $CaCl_2$) were added to a beaker under constant stirring at 60 °C. The amount of enzyme (5 mg) was previously diluted in a buffer solution. After 210 min, 2 mL of the buffer solution and the diluted enzyme solution were added. Thereafter, organosilane (5.5×10^{-4} M) was added. The system was stirred for 30 additional minutes. Gelling occurred sooner than 4 h from the start of the reaction.

Once the sol–gel was finished, the solids were kept at ~50 °C in an oven for 12 h. Thereafter, they were kept at room temperature. Saccharification tests were always carried out on the same day of solvent removal.

2.3 Characterization of the immobilized enzymes

2.3.1 Nitrogen adsorption (Brunauer–Emmett–Teller (BET) and Barret–Joyner–Halenda (BJH) methods)

The surface area, pore size, and total porous volume of the immobilized enzymes were evaluated based on the nitrogen adsorption–desorption isotherms obtained at −196 °C. Approximately 100–200 mg of dry sample was used. The samples were previously degassed at 110 °C for 18 h under vacuum in a MicromeriticsVacPrep 061 instrument. The physical nitrogen adsorption isotherms per sample were obtained using a MicromereticsTriStar II 3020 instrument in the partial pressure range of $0.01 < P_0^{-1} < 0.25$. The surface area (S_{BET}) was calculated by the BET method, while the pore size and total porous volume were obtained using the desorption isotherm according to the BJH method.

2.3.2 Small-angle X-ray scattering (SAXS) measurements

SAXS data were collected in a Nano-inXider (UFRGS Nanoscience and Nanotechnology Center), model S with accessories. This instrument allows a total flow of ~100 mph/s with a resolution that varies in the range of 200–800 μm, an exposure time of 60 s and an overlap between the calibrated and measured curves. Several measurements are made, and then a file is generated containing the average value. Data analysis was performed using the Irena [21] evaluation routine implemented in the IgorPro program (WaveMetrics, Portland, USA) [22].

2.3.3 Fourier transform infrared spectroscopy (FT-IR)

The infrared molecular absorption spectra of the matrices (without enzyme) were analyzed using a Shimadzu FTIR-8300 spectrophotometer with a DLaTGS detector (standard deuterated L-alanine doped triglycine sulfate) in the range of 4000–400 cm^{-1} with a resolution of 4 cm^{-1} in transmission mode. The samples were mixed with dry KBr and analyzed as pellets.

2.3.4 Scanning electron microscopy (SEM)

SEM experiments were carried out using a BOI-SEM-10 microscope. The samples were initially attached to a carbon tape and then coated with carbon by conventional spray techniques. Analyses carried out at the UFRGS electronic microscopy center.

2.4 Evaluation of immobilized enzyme catalytic activity in starch saccharification

Based on a previous study [20], the following optimized conditions were then applied in the present study (Supplementary Table 1).

In a typical experiment, a 100-mL suspension in deionized water was prepared consisting of sodium acetate (2.5 mmol), calcium chloride (0.5 mmol), and starch (1 g). Saccharification with encapsulated α-amylase from *Aspergillus oryzae* and β-amylase demanded first starch solution heating at 70 °C for dissolution, followed by cooling the reaction back to 50 °C and 45 °C, respectively. Then, the

immobilized enzyme was added to the reaction system. In the case of immobilized α-amylase from *Bacillus subtilis*, the operating temperature (65 °C) was enough to dissolve the starch. After 60 min of reaction time, the reaction was ceased, and a 0.5-mL aliquot was removed and submitted to an enzyme-deactivation process (close to 100 °C) and later used for DNS tests. Part of the must was frozen for later analyses.

2.5 Methods of analysis of the resulting sugars

The quantitative determination of the reducing sugars was carried out according to the DNS method developed by Miller [23]. A standard curve was drawn upon measuring the absorbance at 540 nm. Since glucose standard solutions are susceptible to absorbance changes, a new calibration curve was prepared daily. An example of a typical curve is described by the following equation: $y = 0.5068\times + 0.0346$ and $r^2 = 0.9905$.

The quantification of maltose and glucose was carried out by HPLC. The equipment was an Ultimate 3000 Dionex and refractive index detector (RID) Shodex RI-101. HPLC separation was carried out on a Luna® Omega Sugar column (150 × 4.6 mm × 3 µm) at 40 °C, with an isocratic mobile phase of CH_3CN:H_2O 75:25, maintained at a flow rate of 1.0 mL min^{-1}. The sample solutions were filtered through 0.45-µm membrane filters, and the injection volume was 20 µL. The temperature of the RID was kept at 40 °C.

Linearity was established by triplicate injections of seven different standard concentrations (50, 100, 200, 300, 500, 700, and 1000 µg mL^{-1}). The chromatographic peaks corresponding to glucose and maltose were matched with the retention time of the standard. Good linearity ($r^2 = 0.999$ for glucose and 0.999 for maltose) was obtained with regression equations of $y = 0.0024\times + 0.0228$ and $y = 0.0022\times - 0.0052$ for glucose and maltose, respectively.

3 Results and discussion

3.1 Characterization of the immobilized systems

Attempts to characterize the grafted systems by X-ray photoelectron spectroscopy were not successful. Perhaps the grafted enzyme content was below the sensitivity of the technique or the enzyme lain in the bulk of the particle, which in turn may explain both its not detection and its lower activity.

3.1.1 Surface area and porosity

The resulting encapsulated enzymes were initially analyzed in terms of textural properties. Figure 1 illustrates some examples of selected nitrogen adsorption isotherms.

Almost all the encapsulated systems exhibited a type-IV isotherm profile. In type-IV isotherms, two distinct branches are observed: the lower branch shows the amount of gas adsorbed with increasing relative pressure, while the upper branch represents the amount of gas desorbed in the reverse process. These isotherms are characteristic of mesoporous and macroporous solids, in which the evaporation process is different from the condensation process [24]. The different paths characterize a hysteresis between the adsorption and desorption processes. Similar results have been reported in the case of silica sol–gel-based encapsulation systems prepared by sol–gel processes such as immobilized trypsin and pepsin enzymes [25], carbonic anhydrase, and horseradish peroxidase [26] or lipase [27].

It is worth mentioning that the sole system that exhibited a different isotherm profile is that using [3-(2-aminoethylamino) propyl] organosilane in the case of the immobilization of bacterial α-amylase. In this case, a type-II isotherm is observed (Supplementary Fig. 1). This isotherm type is characteristic of nonporous or macroporous adsorbents [24].

Table 1 presents the results extracted from the nitrogen adsorption isotherm parameters.

Considering the data presented in Table 1, it can be noted that the use of organosilanes causes a decrease in surface area in the majority of the systems compared to immobilization within bare silica (without organosilane). A few systems exhibit a slight increase in surface area.

The total porous volume also decreases in most samples. The pore diameter increases significantly in most cases. Therefore, in general, organosilanes reduced the specific area and total porous volume, in addition to promoting a relevant increase in the average pore size *n*.

Attempts to correlate textural parameters and biocatalytic activity do not provide sharp correlations. A strong Spearman correlation is observed in the case of surface area and the reducing sugar concentration for the three investigated amylases in the case of alkyl-modified organosilanes (Fig. 2).

Such results suggest that the effect on the sugar reducing content is not solely dependent on textural properties but on the interaction between the organosilane and the enzyme catalyst sites. The systems were further analyzed by SAXS.

3.1.2 Textural parameters from SAXS analyses

The SAXS profile of the samples (not shown) suggests the existence of two levels. Table 2 presents the results obtained from curve fittings performed using IgorPro software.

SAXS is capable of characterizing the size distribution and aggregation status of nanoparticles; therefore, it is widely applied to analyze silica nanoparticles. The SAXS curves of the encapsulated enzymes reveal that the systems have average diameters of 183 nm (bacterial α-amylase), 189 nm (fungal α-amylase), and 173 nm (beta amylase).

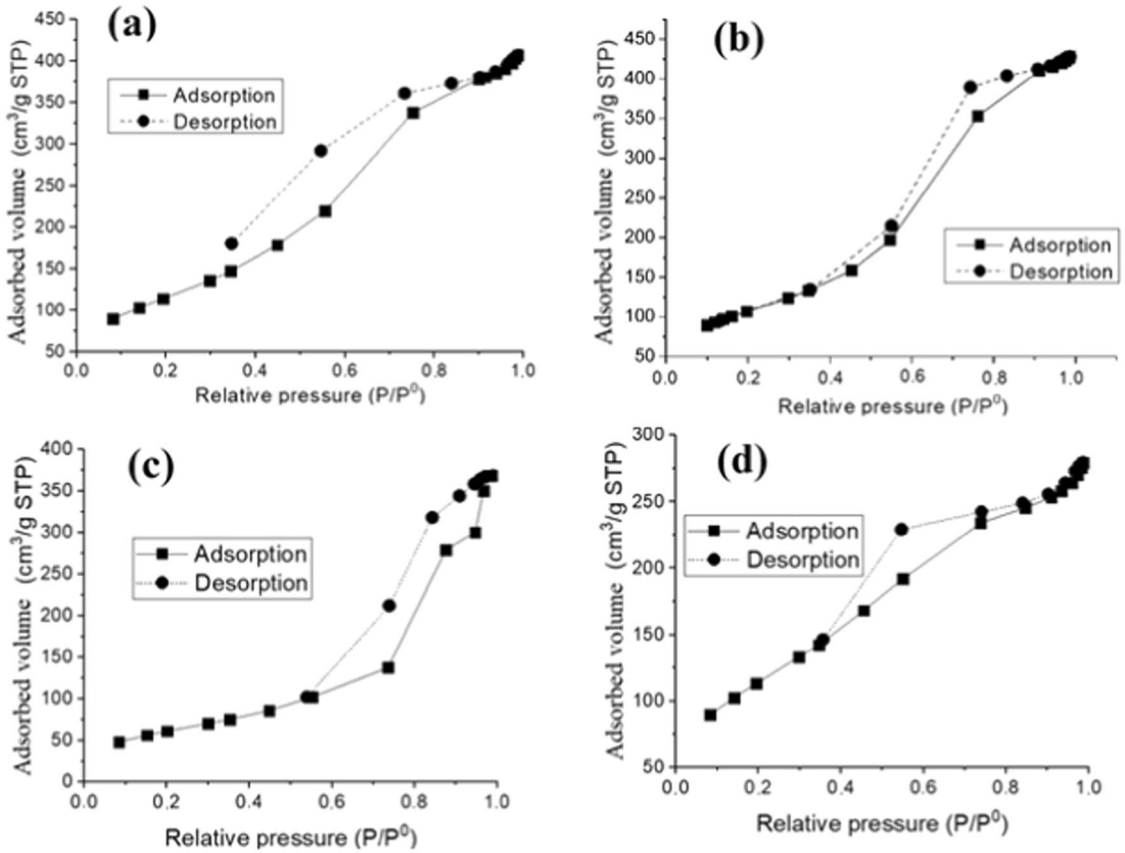

Fig. 1 Examples of nitrogen adsorption isotherms obtained from immobilized bacterial α-amylase and β-amylase. **a** Bacterial α-amylase with triethoxymethylsilane, **b** bacterial α-amylase with N-octyltriethoxy-silane, **c** β-amylase with [3-2-aminoethylamino)propyl]trimethoxysilane, and **d** β-amylase with [1-(3-trimethoxsilyl) propyl]urea

Table 1 Textural parameters extracted from nitrogen adsorption analysis for α and β-amylase

Organosilane	α-amylase (*Bacillus subtilis*)			α-amylase (*Aspergillus oryzae*)			β-amylase		
	S_{BET} (m^2/g)	P_v (cm^3/g)	P_d (Å)	S_{BET} (m^2/g)	P_v (cm^3/g)	P_d (Å)	S_{BET} (m^2/g)	P_v (cm^3/g)	P_d (Å)
None (Silica)	391	0.67	45.2	310	0.56	48.8	554	0.63	32
C1 (Triethoxymethylsilane)	430	0.701	58.1	402	0.054	53.5	497	0.575	43.3
C8 (*N*-octyltriethoxysilane)	368	0.536	55.1	319	0.061	53.0	413	0.303	51.3
C18 (Trimethoxy-octadecylsilane)	310	0.577	70.2	-	-	-	-	-	-
(3-Aminopropyl)triethoxysilane	350	0.524	50.4	343	0.123	60.4	246	0.102	110.2
[1-(3-Trimethoxsily)propyl]urea	314	0.205	48.7	454	0.427	33.4	422	0.395	40.6
[3-(2-Aminoethylamino)propyl] Trimethoxysilane	266	0.270	96	315	0.134	98	-	-	-
N^1-(3-Trimethoxsilylpropyl)diethylenetriamine	232	0.572	119.1	-	-	-	-	-	-
(3-Mercaptopropyl)trimethoxysilane	164	0.0125	38.9	290	0.063	89	-	-	-

S_{BET} specific area, *Vp* total porous volume, *Dp* Pore diameter, -unvalued

In addition, according to Table 2, no clear trend can be observed regarding primary particle size (Rg1). The addition of organosilane later during synthesis may not affect the primary particles that have already formed.

Gels generally have aggregate structures that behave like a mass fractal structure. Parameter *P* can be obtained by tilting the line resulting from the graph dialog I (q) versus q. The parameter *P*, in the range $1 < P < 3$, is a measure of the cluster mass fractal dimension [28]. In the range $3 < P < 4$, the values are associated with the surface fractal dimension. The Px coefficients are associated with the slope of the curve within the linear region obtained by SAXS curve, which may provide particle shape information.

Some strong correlations were found between the SAXS data and biocatalytic activity, namely, (i) $r_{Sp} = 0.912$ ($p < 0.01$) positive correlation between P_1 and reducing

sugar content, i.e., the less ramified the particles are, the higher the catalyst activity. Conversely, two strong indirect correlations are noted: (ii) $r_{Sp} = -0.975$ ($p < 0.01$) correlation between the radius of gyration and reducing sugar content and (iii) $r_{Sp} = -0.872$ ($p < 0.05$) correlation between P_2 and reducing sugar content, i.e., the lower the particle radius of gyration and the higher the degree ramification of the secondary particles, the higher the catalyst bioactivity is.

3.1.3 Structural characterization by FT-IR analysis

The samples were subjected to FT-IR analysis. The silica network formation is characterized by a set of bands. The broadband centered at 1080 cm^{-1} is characteristic of the vibration modes of asymmetric Si–O stretching. The band close to 967 cm^{-1} is associated with Si–O–Si angular deformation. The band close to 800 cm^{-1} is related to the symmetrical stretching of the Si–O bond. The band at 470 cm^{-1} is related to deformation (Si–O–Si) [29–33].

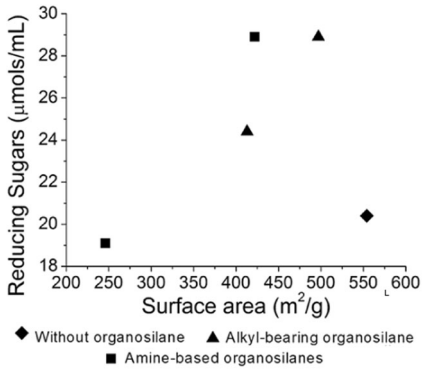

Fig. 2 Correlation between surface area and reducing sugars of enzymes encapsulated with alkyl-bearing organosilane

Chemical groups from the organosilanes attached to the hybrid materials could be observed in the region between 3000 and 2700 cm^{-1}. One of the peculiarities observed is in the sample containing C18, whose spectrum contains two peaks related to alkyl chains, assigned to asymmetrical stretching $\left[\nu_{as\ ((C)-CH_2)}\right]$ and the symmetrical mode $\left[\nu_{s((C)-CH_2)}\right]$ at 2926 and 2855 cm^{-1}, respectively [34].

Specifically, in the case of C18, models consider crystalline-state positions in which the long chains are fully extended with an all-*trans* conformation and the liquid state, in which the chains are randomly oriented. The $\nu_s(CH_2)$, $\nu_{as}(CH_2)$, and $\nu_{as}(CH_3)$ are selected for structural interpretation owing to the minimal overlap of their absorption bands with those of other modes. For instance, according to the literature [35], the position of these peak frequencies provides insight into the intermolecular environment of the alkyl chains in these assemblies. The peak position for the $\nu_{as}(CH_2)$ mode of a crystalline polymethylene chain (2920 cm^{-1}) is 8 cm^{-1} lower than that for the liquid state (2928 cm^{-1}). In the present hybrid system, such bands are centered at 2926 and 2855 cm^{-1}, suggesting a liquid state position. Silicas with this type of arrangement can facilitate the diffusion of substrate and reagents. Nevertheless, in the present study, the presence of such a long alkyl chain causes a reduction in catalyst activity (see Table 1), probably due to the mobility of such groups (in liquid-like conformation), which in turn may have deactivated or blocked access to the catalyst activity sites. Further studies are necessary to evaluate the effect of alkyl-chain conformation (controlled at different encapsulation conditions) on catalyst bioactivity. A broader analysis of the FT-IR peaks is available in the previous article [20].

Table 2 Curve fit results performed on IgorPro obtained from SAXS samples

	α-amylase (*Bacillus subtilis*)			α-amylase (*Aspergillusoryzae*)			β-amylase		
Organosilane	Rg1 (nm)	P1	P2	Rg1 (nm)	P1	P2	Rg1 (nm)	P1	P2
None	187.4	4.00	2.8	207.5	4.00	1.88	166.5	4.00	1.77
C1 (Triethoxymethylsilane)	185.8	3.47	1.4	201.1	4.00	1.67	159.7	4.00	1.56
C8 (*N*-octyltriethoxysilane)	132.6	3.16	3.7	170.0	4.00	1.68	165.4	4.00	1.88
C18 (Trimethoxy-octadecylsilane)	156.1	3.33	3.0	-	-	-	-	-	-
(3-Aminopropyl)triethoxysilane	256.0	3.47	2.2	160.6	3.73	1.47	264.0	3.50	2.00
[1-(3-Trimethoxysily)propyl]urea	192.1	3.65	2.3	172.3	4.00	1.54	112.6	3.64	1.58
[3-(2-Aminoethylamino)propyl] trimethoxysilane	117.4	1.56	3.6	235.7	3.74	2.08	-	-	-
N^1-(3-Trimethoxysilylpropyl) diethylenetriamine	241.2	3.05	2.5	-	-	-	-	-	-
(3-Mercaptopropyl) trimethoxysilane	181.3	3.55	2.3	175.2	3.85	1.98	-	-	-

- not determined

3.1.4 Scanning electron microscopy (SEM)

Figure 3 illustrates a representative SEM micrograph corresponding to encapsulated bacterial alpha-amylase. The resulting silica-based materials have wrinkled surface formed by small spherical aggregates measuring ca. 100 µm.

3.2 Effect of the nature of organosilane on starch saccharification

Table 3 presents the results of the determination of reducing sugars by the DNS method for the immobilized amylase in the presence of organosilanes. For comparative reasons, an encapsulated system within bare silica was also included.

Enzymes have a pH range in which their activity is maximal: at higher or lower pH, the activity decreases. This is due to the effect of pH on several factors, namely, (i) substrate binding to the enzyme, (ii) ionization state of amino acid residues involved in the catalytic activity of the enzyme, (iii) substrate ionization, and (iv) protein structure alteration [14]. Therefore, analyses of the data reported in Table 3 have to take into account the optimized biocatalytic activity of the three enzymes at different pH and temperature ranges. Analyses of the reducing sugar content of the immobilized enzymes without the presence of organosilanes show that the conversion to sugars decreases (by 30.5, 25.5, and 20.4 µmol/mL) for fungal α-amylase, bacterial α-amylase, and β-amylase, respectively. Therefore, all the performed analyses should consider these differences.

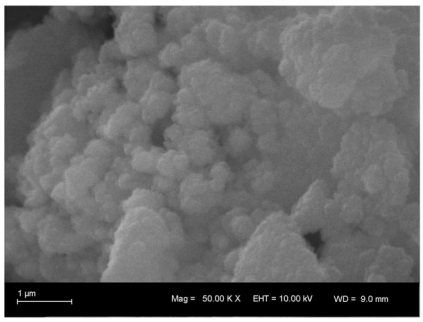

Fig. 3 Micrograph obtained by scanning electron microscopy (SEM) of encapsulated bacterial alpha-amylase

The results shown in Table 3 are consistent with comparative studies of starch degradation between α-amylase and β-amylase reported in the literature. α-amylase is more efficient than β-amylase, generating a higher concentration of reducing sugars, as already cited in other studies [36]. The values associated with fungal α-amylase immobilization are scattered. There seems to be a greater randomization in the results for the immobilization of this enzyme.

The three investigated enzymes seem to be affected by the presence of most of the studied organosilanes. Bacterial α-amylase is shown to be robust (see, for instance, C1 or S-based organosilane). In spite of this, some of the compounds caused reduction in the catalytic activity. It is worth noting the effect of (N1-(3-trimethoxysilylpropyl)diethylenetriamine), which caused an increment in reducing sugar production. Conversely, the catalyst activity of *Aspergillus oryzae* α-amylase is shown to be sensitive to the presence of organosilane, which, in some cases, significantly decreased the reducing sugar production. A positive effect is observed in the case of β-amylase, in which an increase in catalyst activity is observed for most of the added organosilanes. It is worth noting that the molecular size of the enzyme and substrate interferes with the diffusion of reagents and products. According to the literature, α-amylase is larger in size than β-amylase. Maize malt characterization shows that α- and β-amylase have molecular weights of 67.4 and 47.5 kDa, respectively [37]. Therefore, the lower molecular weight of β-amylase could make it more prone to organosilane effects. In addition, one cannot neglect the structural

Table 3 Reducing sugar content obtained from musts resulting from starch hydrolysis using immobilized amylase

Organosilane	Reducing sugar (µmols/mL)		
	α-amylase (*Bacillus subtilis*)	α-amylase (*Aspergillus oryzae*)	β-amylase barley
None	25.5	30.5	20.4
C1 (Triethoxymethylsilane)	25.4	29.6	28.9
C8 (*N*-octyltriethoxysilane)	21.8	26.5	24.4
C18 (Trimethoxy-octadecylsilane)	17.8	-	-
(3-Aminopropyl)triethoxysilane	23.6	6.1	19.1
[1-(3-Trimethoxysily)propyl]urea	24.9	27.6	28.9
[3-(2-Aminoethylamino)propyl]	20.4	11.5.	-
N^1-(3-Trimethoxysilylpropyl) diethylenetriamine	28.6	-	-
(3-Mercaptopropyl)trimethoxysilane	23.7	26.5	-

- not determined

differences between α- and β-amylase peptide chains [38]: the α helix has a rod-like shape, which is stabilized by hydrogen bridges between the NH and CO clusters of the main chain, represented as twisted ribbons or rods. The β structure differs greatly from that of the α helix: it is composed of two or more peptide chains, with the β strip almost fully distended rather than tightly wound; a β sheet is formed by joining two or more β filaments by hydrogen bridges [39]. Therefore, the differences in reducing content may also be assigned to the structural differences between α-amylase and β-amylase.

Considering the alkyl-containing organosilanes (C1, C8, and C18), there appears to be a linear trend between the silane size (length chain) and conversion to reducing sugars: the longer the alkyl chain is, the lower the reducing sugar capacity. These results diverge from those reported in the literature for encapsulated lipase in which increasing the chain length of alkyl groups improved specific activity (substrate mg per unit of time) and the total activity of immobilized lipase [40]. Several trend has been reported in the case of immobilized lipase on alkyl silane modified magnetic nanoparticles [41]. Comparison here has to be taken with caution. In the case of amylase, substrate (starch) and products (sugars) are hydrophilic, while lipid involved in the case of lipase is hydrophobic. Thus diffusion through the pores is affected by their hydrophilicty/hydrophobocity. In the case of immobilized lipase, activity increasing with increasing alkyl-chain length was assigned to the improvement of hydrophopic interactions. In the present case, it seems that the mobility of the alkyl chain may block or interact with the active sites of the enzymes, impinging a reduction in its catalytic activity. In addition, one cannot neglect that there is a relevant structural difference between amylases and lipase. In the lipase there is a helicoid oligopeptide that covers the active center, named "lid," which in turn render more complex the access of substrates to its catalytic center [42]. Such mechanism is absent in the case of lipase.

According to Table 3, the system containing mercaptansilane showed slightly lower values than that obtained without the use of silanes. Thus, it seems that this functional group does not appear to have a denaturing effect on the enzyme. Such behavior is consistent with cellulase immobilization with 3-mercaptopropyl-trimethoxysilane functionalization reported in the literature [12]. In that study, the role of the organosilane may have been to work as spacer setting the catalyst site farther from the formed silica surface, in turn improving the accessibility of the substrate to the catalyst centers, as reported in the case of silica-based immobilized lysozyme [43].

To better understand the comparative behavior observed among the three encapsulated systems, the hybrid-supported enzymes were further characterized by a set of complementary analytical techniques to extract potential textural and structural effects on the resulting encapsulated enzymes.

3.3 Glucose and maltose concentration (HPLC)

Table 4 presents the results obtained by the analysis of musts obtained from starch saccharification by HPLC, expressed in terms of glucose and maltose concentrations.

According to Table 4, generally, the use of organosilanes decreases maltose concentrations in musts resulting from saccharification. The glucose concentrations have more random values. Taking into account the nature of the alkyl-organosilanes, it is possible to state that there is a differentiated relation between glucose and maltose concentration and the length of the carbon chain of organosilanes.

The use of organosilanes in the encapsulation of fungal α-amylase causes an increase in glucose concentration during saccharification in most cases, with two exceptions: [3-(2-aminoethylamino)propyl]trimethoxysilane causes a sharp decrease in glucose concentration (33.4 mg/L) and (3-aminopropyl) triethoxysilane with a subtle reduction in glucose concentration (389 mg/L). On the other hand, the concentration of maltose decreases for all the tested organosilanes.

Therefore, in general, the use of organosilanes favors the generation of glucose over the generation of maltose, i.e., an increase in the glucose/maltose ratio. Apparently, starch cleavage by β-amylase during saccharification is somewhat affected by the presence of organosilanes around the catalyst centers.

Correlating the glucose/maltose ratio and the porosity results, it is possible to find a high correlation in the case of β-amylase and its properties: surface area ($r_{Sp} = 0.71$, $p < 0.05$), total porous volume ($r_{Sp} = 0.75$, $p < 0.05$), and pore diameter ($r_{Sp} = 0.93$, $p < 0.05$), which corroborates the rationale for the effect of pore size on the generation of maltose. α-amylase is an enzyme that generates glucose and maltose. β-amylase generates maltose [44]. In the present study, the addition of organosilanes tends to increase the glucose/maltose ratio. It seems that more confined sites (smaller surface area and smaller total porous volume) affect the catalyst centers.

It is worth noting that there are industrial processes that seek to maximize glucose production: higher glucose may represent higher production in fermentative processes. Then, in some branches of the biochemistry industry, immobilization of amylases that maximize the proportion of glucose may be attractive.

4 Conclusion

In the present study, in which organosilane is included in amylase silica matrix encapsulation, the molecular size of the organosilanes affects the porosity of the resulting immobilized systems: larger organosilanes tend to generate

Table 4 HPLC glucose and maltose concentrations obtained from the immobilized amylase saccharification tests

Organosilane	α-amylase (*Bacillus subtilis*)			α-amylase (*Aspergillusoryzae*)			β-amylase		
	Glucose mg/L	Maltose mg/L	G/M	Glucose mg/L	Maltose mg/L	G/M	Glucose mg/L	Maltose mg/L	G/M
None	1245	3031	0.41	408	5501	0.074	69	5011	0.014
C1 (Triethoxymethylsilane)	879	1329	0.66	578	3833	0.151	31	4875	0.006
C8 (*N*-octyltriethoxysilane)	991	1104	0.90	599	4064	0.147	165	4937	0.033
C18 (Trimethoxy-octadecylsilane)	1233	884	1.39	-	-	-	-	-	-
(3-Aminopropyl)triethoxysilane	1453	1113	1.31	389	538	0.723	387	3194	0.121
[1-(3-Trimethoxysily)propyl]urea	824	1131	0.73	1103	3992	0.276	603	4807	0.125
[3-(2-Aminoethylamino)propyl]	719	971	0.74	33.4	1214	0.028	-	-	-
N^1-(3-Trimethoxysilylpropyl)diethylenetriamine	1340	928	1.44	-	-	-	-	-	-
(3-Mercaptopropyl)trimethoxysilane	945	849	1.11	569	3202	0.178	-	-	-

- not determined

a silica-based matrix with a larger specific area and larger total porous volume. On the other hand, the increase in porosity affects the biocatalytic activity of encapsulated enzymes: there is a correlation between surface area/total porous volume and reducing sugar content.

The nature of the amylase also seems to be affected by the nature of the added organosilane. β-amylase is one of the encapsulated systems that appears to have been most affected in the way starch is broken down, with an increase in reducing sugar with the use of organosilanes.

The addition of organosilanes tends to increase the glucose/maltose ratio. In industrial processes that seek to maximize glucose production, the use of organosilane-encapsulated enzymes is a viable and promising alternative. Glucose is the most rapidly consumed carbohydrate in fermentation. Thus, obtaining a higher glucose yield from starch may represent optimization in further industrial processes.

Acknowledgements This work was financed by CNPq (Project # 310408/2019-9). FAPERGS (Project 19/2551-0001869-0) is also thanked.

Compliance with ethical standards

Conflict of interest The authors declare that they have no conflict of interest.

References

1. Basso A, Serban S (2019) Industrial applications of immobilized enzymes—a review. J Mol Catal 479:110607
2. Ren S, Li C, Jiao X, Jia S, Jiang Y, Bilal M (2019) Recent progress in multienzymes co-imobilization and multienzyme system applications. Chemical Eng J 373:1254–1278
3. Thompson MP, Peñafiel I, Cosgrove SC, Turner NJ (2019) Biocatalysis using immobilized enzymes in continuous flow for the synthesis of fine chemicals. Org Process Res Dev 23:9–18
4. Virgen-Ortíz JJ, Pedrero SG, Fernandez-Lopez L, Lopez-Carrobles N, Gorines BC, Otero C (2017) Desorption of lipases immobilized on octyl-agarose beads and coated with ionic polymers after thermal inactivation. Stronger adsorption of polymers/unfolded protein composites. Molecules 22:91–102
5. Salgaonkar M, Nadar SS, Rathod VK (2018) Combi-metal organic framework (Combi-MOF) of α-amylase and glucoamylase for one pot starch hydrolysis. Int J Biol Macromol 13:464–475
6. Talekar S, Pandharbale A, Ladole M, Nadar S, Mulla M, Japhalekar KP, Arage D (2013) Carrier free co-immobilization of alpha amylase, glucoamylase and pullulanase as combined cross-linked enzyme aggregates (combi-CLEAs): a tri-enzyme biocatalyst with one pot starch hydrolytic activity. Bioresour Technol 147:269–275
7. Graebin NG, Schöffer JD, Andrades DD, Hertz PF, Ayub MA, Rodrigues RC (2016) Immobilization of glycoside hydrolase

families GH1, GH13, and GH70: state of the art and perspectives. Molecules 21(8):21081074
8. Valldeperas M, Salis A, Barauskas J, Tiberg F, Arnebrant T, Razumas V, Monduzzi M, Nylander T (2019) Enzyme encapsulation in nanostructured self-assembled structures: toward biofunctional supramolecular assemblies. Curr Opin Colloid Interface Sci 44:130–142
9. Drout RJ, Robinson L, Farha OK (2019) Catalytic applications of enzymes encapsulated in metal-organic frameworks. Coord Chem Rev 381:151–160
10. Singh K, Mishra A, Shama D, Singh K (2019) Nanotechnology in enzyme immobilization: an overview on enzyme immobilization with nanoparticle matrix. Curr Nanosci 15:234–241. Bentham Science Publishers
11. Nadar SS, Rathod VK (2018) Magnetic-metal organic framework (magnetic-MOF): a novel platform for enzyme immobilization and nanozyme applications. Int J Biol Macromol 120:2293–2302
12. Adhikari BR, Schraft H, Chen A (2017) A high-performance enzyme entrapment platform facilitated by a cationic polymer for the efficient electrochemical sensing of ethanol. Analyst 142:2595–2602
13. Lima U de A (2019) Industrial biotechnology—fermentative and enzymatic processes, Publishing company, Brochura
14. Levy D, Zayat M (2015) The sol-gel handbook: synthesis, characterization and aplications. Wiley-VCH, Weinheim, Germany
15. Neslcon DL, Cox MM (2017) Lehninger, principles of biochemistry., 7th edn. W. H. Freeman & Co, New York
16. Voet D, Voet JG, Pratt CH (2011) Fundamentos de bioquímica, 4th edn. John Wiley & Sons, Hoboken
17. Evstatieva Y, Yordanova M, Chernev G, Ruseva Y, Nikolova D (2014) Sol-gel immobilization as a suitable technique for enhancement of α-amylase activity of Aspergillus oryzae PP. Biotechnol Biotechnol Equip 28:728–732
18. Singh V, Singh D (2014) Diastase α-amylase immobilization on sol–gel derived guar gum-gelatin-silica nanohybrid. Adv Mater Lett 5:17–23
19. Vera-Avila LE, Morales-Zamudio E, Garcia-Camacho MP (2004) Activity and reusability of sol-gel encapsulated α-amylase and catalase, performance in flow-through systems. J Sol-Gel Sci Technol 30:197–204
20. Fernandez Caresani JR, Dallegrave A, dos Santos JHZ (2020) Amylases imobilization by sol-gel entrapment: aplication for starch hydrolysis. J Sol-Gel Sci Technol 94:229–240
21. Ilavskyand J, Jemian PR (2009) Irena: tool suite for modeling and analysis of small-angle scattering. J Appl Cryst 42:347–353
22. Kline SR (2206) Reduction and analysis of SANS and USANS data using IGOR Pro. J Appl Cryst 39:895–900
23. Miller GL (1959) Use of dinitrosalicylic acid reagent for determination of reducing sugar. Anal Chem 31:426–428
24. K.S.W, Sing (1982) Reporting physisorption data for gas/solid systems. Pure Appl Chem 54:2201–2218
25. Kato K, Kawachi Y, Nakamura H (2014) Silica–enzyme–ionic liquid composites for improved enzymatic activity. J. Asian Ceram Soc 2:33–40
26. Gößl D, Singer H, Chiu H, Schmidt A, Lichtnecker M, Engelk H, Bein T (2019) Highly active enzymes immobilized in large pore colloidal mesoporous silica nanoparticle. New J Chem 43:1671–1680
27. Barbosa AS, Lisboa JA, Silva MA, Carvalho NB, Pereira MM, Fricks AT, Mattedi S, Lima ÁS, Franceschi E, Soares CMF (2016) The novel mesoporous silica aerogel modified with protic ionic liquid for lipase immobilization. Quim Nova 39:415–426.
28. Lee S, Fischer TB, Stokes MR, Klingler RJ, Ilavsky J, McCarty DK, Wigand MO, Derkowski A, Winans RE (2014) Dehydration effect on the pore size, porosity, and fractal parameters of shale rocks: ultrasmall-angle X-ray scattering study. Energy Fuels 28 (11):6772–6779
29. Brinker JC, Scherer GW (1990) Sol-gel science, the physics and chemistry of sol-gel processing. Elsevier Science, San Diego
30. Colthup NB (1990) Introduction to infrared and Raman spectroscopy, 3rd edn. Academic, San Diego
31. Vansant EF, Van Der VP, Vrancken KC (1995) Studies in surface science and catalyst. In: Characterization and chemical modification of the silica surface, vol. 92. Elsevier, Amsterdam
32. Nakamoto K (1997) Infrared and Raman spectra of inorganic and coordination compounds, 5th edn. John Wiley, New York
33. Saikia BJ, Parthasarathy G (2010) Fourier transform infrared spectroscopic characterization of kaolinite from Assam and Meghalaya, Northeastern India. J Mod Phys 1:206–210
34. Fidalgo A, Ciriminna R, Lopes L, Pandarus V, Béland F, Ilharco LM (2013) The sol-gel entrapment of noble metals in hybrid silicas: a molecular insight. Chem Cent J 7:161
35. Snyder RG, Maroncelli M, Strauss HL, Hallmark VM (1986) Temperature and phase behavior of infrared intensities: the poly (methylene) chain. J Phys Chem 90:5623–5630
36. Elif S, Takahiko H, Motoyasu A, Bunzo M (2000) Comparison of degradation abilities of α- and β-amylases on raw starch granules. Process Biochem 35:711–715
37. Biazus JPM, Souza RR, Marquez JE, Franco TT, Santana JCC, Tambourgi EB (2009) Production and characterization of amylases from Zea mays malt. Braz Arch Biol Technol 52:991–1000
38. Pauling L, Corey RB, Branson HR (1951) The structure of proteins: two hydrogen-bonded helical configurations of the polypeptide chain. PNAS 37:205–211
39. Berg JM, Stryer L, Tymoczko JL (2014) Biochemistry, 7th edn. W. H. Freeman & Co., Houndmill
40. Jiangke Y, Liying L, Xiongwen C (2010) Combination of bioimprinting and silane precursor alkyls improved the activity of sol–gel-encapsulated lipase. Enzyme Microb Technol 46:257–261
41. Wang J, Meng G, Tao K, Feng M, Zhao X(2012) Immobilization of lipases on alkyl silane modified magnetic nanoparticles: effect of alkyl chain length on enzyme activity. Plos ONE 7(8):e43478
42. Brzozowski A, Savage H, Verma CH, Turkenburg J, Lawson D, Svendsen A, Patkar S (2001) Structural origins of the interfacial activation in thermomyces (Humicola) lanuginosa lipase. Biochemistry 39:15071–15082
43. Ramanathan M, Luckarift HR, Sarsenova A, Wild JR, Ramanculov EK, Olsen EV, Simonian AL (2009) Lysozyme-mediated formation of protein–silica nano-composites for biosensing applications. Coll Surf B: Biointerfaces 73:58–64
44. Campbell MK, Farrell SO (2015) Biochemistry, 8th edn. Cengage Learning, Standford